Journal of the Korean Physical Society (2024) 85:371–380
https://doi.org/10.1007/s40042-024-01133-4

Online ISSN 1976-8524
Print ISSN 0374-4884

ORIGINAL PAPER - FLUIDS, PLASMA AND PHENOMENOLOGY

In-vacuum undulators for the first phase beamlines of Korea-4GSR

Changwan Ha[1] · Ik Seon Kwon[1] · Ki-Jeong Kim[1] · Jehan Kim[1] · Jae-Hong Lim[1]

Received: 19 March 2024 / Revised: 16 May 2024 / Accepted: 12 June 2024 / Published online: 31 July 2024

Abstract
Korea-4GSR, a new synchrotron radiation facility currently under construction in Ochang, Chungbuk, South Korea, introduces three types of in-vacuum undulators (IVUs) for its first phase hard X-ray beamlines: IVU20, IVU22, and IVU24. These IVU types share a common 3-m-long framework capable of adjusting the magnetic gap size between 5 and 18 mm, but they differ in the undulator period length (λ_u). This study characterizes their photon beams in terms of brightness, spectral coverage, source size, angular divergence, coherent fraction, coherent flux, and total and central cone radiation powers, using undulator calculations. The three IVU types are comparable in brightness. IVU20 is the most coherent, although lacking spectral continuity at around 7.5 keV. IVU22 and IVU24 ensure spectral continuity, but their coherent flux is moderately compromised. The performance of the undulators is assessed in comparison to the Pohang Light Source-II (PLS-II) undulator and the U21 undulator at Advanced Photon Source Upgrade (APS-U).

Keywords Korea-4GSR · Synchrotron radiation · In-vacuum undulator · Flux · Coherence

1 Introduction

The Korea fourth-generation storage ring (Korea-4GSR) is a new synchrotron radiation facility under construction in Ochang, Chungbuk, South Korea [1]. It is designed as a multipurpose synchrotron radiation source that aims to achieve both academic excellence and industrial benefits, as is exemplified by the operation models of SPring-8 in Japan and ESRF in France [2, 3]. The facility will operate at an electron energy of 4 GeV, which can produce a wide range of X-rays from soft to hard X-rays. The target emittance is 62 pm rad, which is about 100 times smaller than the emittance of the Pohang Light Source-II (PLS-II) in South Korea. This target is comparable to those of the upgrade project of ESRF-EBS (Extremely Brilliant Source; 130 pm rad) and the Advanced Photon Source Upgrade (APS-U; 75 pm rad) in the USA [4, 5].

✉ Jehan Kim
jehan@postech.ac.kr

✉ Jae-Hong Lim
limjh@postech.ac.kr

[1] Beamline Science Team, 4GSR Research Division, Pohang Accelerator Laboratory, Pohang University of Science and Technology (POSTECH), Pohang, Gyeongbuk 37673, Republic of Korea

The ultra-low emittance is best exploited with undulators. Both the electron beam size

$$\sigma_{x,y} = \sqrt{\varepsilon_{x,y}\beta_{x,y}} \tag{1}$$

and the electron beam divergence

$$\sigma_{x',y'} = \sqrt{\varepsilon_{x,y}/\beta_{x,y}} \tag{2}$$

decrease as the emittance value ε decreases. The parameter β is the beta function in the lattice design, and x and y represent the horizontal and vertical directions on the transverse plane, respectively. They are in general larger than the corresponding inherent photon beam size

$$\sigma_r \cong \frac{\lambda_u\sqrt{N}}{4\pi\gamma *} = \frac{\sqrt{2\lambda_n L}}{4\pi} \tag{3}$$

and the photon beam divergence

$$\sigma_{r'} \cong \frac{1}{2\gamma *\sqrt{N}} = \sqrt{\frac{\lambda_n}{2L}}, \tag{4}$$

where λ_u is the undulator period length, N is the number of periods, γ^* is the effective Lorentz factor of the electron beam, L is the undulator length, and λ_n is the nth harmonic wavelength. The ≅ symbol in Eqs. (3) and (4) denotes the

exclusion of a multiplication factor that represents the profile broadening induced by the spread in electron energy [6]. The source size of the photon beam

$$\Sigma_{x,y} = \sqrt{\sigma_{x,y}^2 + \sigma_r^2} \tag{5}$$

and its angular divergence

$$\Sigma_{x',y'} = \sqrt{\sigma_{x',y'}^2 + \sigma_{r'}^2} \tag{6}$$

are, therefore, determined largely by $\sigma_{x,y}$ and $\sigma_{x',y'}$. The ultra-low ε, which reduces $\sigma_{x,y}$ and $\sigma_{x',y'}$ according to Eqs. (1) and (2), also reduces $\Sigma_{x,y}$ and $\Sigma_{x',y'}$, thereby enhancing both the brilliance

$$B = \frac{\text{flux}}{4\pi^2 \Sigma_x \Sigma_{x'} \Sigma_y \Sigma_{y'}}$$

and the coherent fraction

$$F = \frac{(\lambda/4\pi)^2}{\Sigma_x \Sigma_{x'} \Sigma_y \Sigma_{y'}} \tag{7}$$

of the undulator radiation [7]. Earlier, Oh et al. assessed the photon beam characteristics of Korea-4GSR using preliminary machine parameters and assuming an undulator identical to the one from PLS-II [8]. They predicted a beam with

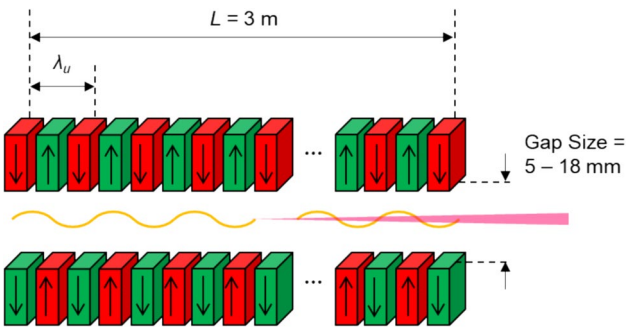

Fig. 1 Schematic of an undulator featuring an undulator period length of λ_u, a total length L (3 m), and the variable gap size. Fast moving electrons experience an alternating magnetic field and wiggle to emit synchrotron radiation as they change direction. These emissions interfere constructively, resulting in the production of undulator radiation

100 times higher brilliance and coherence than the current one at PLS-II.

Recently, the Korea-4GSR project has finalized the specification for undulators in the first phase hard X-ray beamlines. This entails an in-vacuum undulator (IVU) available in three variants: IVU20 with a λ_u of 20 mm, IVU22 with 22 mm, IVU24 with 24 mm. All three IVU types conform to a standardized framework that is 3 m long and can adjust the magnetic gap size between 5 and 18 mm, as illustrated in Fig. 1. The undulator length has been determined to limit its contribution to the total coupling impedance of the storage ring, ensuring storage of high electric currents [9]. Table 1 compares the IVUs with the PLS-II undulator and the U21 undulator at APS-U, which has a similar λ_u. The deflection parameter K in that table is given by

$$K \equiv \frac{eB_0\lambda_u}{2\pi mc} = 0.9337 B_0[\text{T}]\lambda_u[\text{cm}],$$

where B_0 is the magnetic field strength in the midplane that is controlled by the undulator magnetic gap size (referred to as the gap size hereafter).

This study predicts the photon beam characteristics of the three IVU types using the latest machine parameters of Korea-4GSR. They exhibit similar brightness levels, fluctuating within a range of ± 30% throughout the spectral range. IVU20 is the most coherent and least thermal. IVU22 and IVU24 ensure continuous spectral coverage suitable for photon energy scanning applications. The IVUs are more than ten times brighter than the PLS-II undulator with more than 1000 times higher coherent flux. The photon characteristics are comparable to that of the undulator U21 at the APS-U.

2 Experiments and discussion

Table 2 presents the machine parameters used in this study. Compared to PLS-II, Korea-4GSR exhibits significantly smaller electron beam size and divergence. Horizontally, the electron beam size and divergence are reduced by factors of 17 and 10, respectively. Vertically, the reduction factors are 4 and 2.6, respectively. The electron beam size

Table 1 Specifications of undulators compared in this study [4, 8]

Facility	Korea-4GSR			PLS-II	APS-U
Undulator	IVU20	IVU22	IVU24	IVU20	U21
Period length, λ_u (mm)	20	22	24	20	21
Total length (m)	3.0	3.0	3.0	1.3	2.4
Number of periods, N	150	136	125	65	111
Gap size (mm)	5–18	5–18	5–18	6–18	N/A
Deflection parameter, K	1.91–0.22	2.31–0.30	2.74–0.39	1.54–0.22	1.21–0.32

Table 2 Machine parameters of synchrotron radiation facilities selected for this study

	Korea-4GSR	PLS-II	APS-U brightness mode
Electron energy (GeV)	4	3	6
↳ Lorentz factor γ	7828	5870	11,740
Electron energy spread (%)	0.126	0.107	0.130
Current (mA)	400	400	200
Natural emittance ε (pm rad)	62	5800	75
Coupling constant	0.1	0.01	0.1
↳ ε_x (pm rad)	56	5800	68
↳ ε_y (pm rad)	5.6	58	6.8
β_x (m)	6.3	6.5	7.0
β_y (m)	2.8	4.4	2.4
↳ Horizontal beam size σ_x (μm)	19	320	22
↳ Vertical beam size σ_y (μm)	4.0	16	4.1
↳ Horizontal beam divergence $\sigma_{x'}$ (μrad)	3.0	30	3.1
↳ Vertical beam divergence $\sigma_{y'}$ (μrad)	1.4	3.6	1.7

Values derived from the parameters listed above are marked with a symbol (↳) [4, 8]

and divergence are comparable to those of APS-U operating in brightness mode.

To calculate the undulator radiation, we used the SPECTRA software [10, 11]. Undulator radiation consists of discrete harmonics with a narrow spectral bandwidth, which is inversely proportional to N and the harmonic number n:

$$\frac{\Delta\lambda}{\lambda} = \frac{1}{n \cdot N}.$$

The fundamental or first harmonic wavelength λ_1 of the on-axis undulator radiation is given by

$$\lambda_1 = \frac{\lambda_u}{2\gamma*^2} = \frac{\lambda_u}{2\gamma^2}\left(1 + \frac{K^2}{2}\right),$$

where γ is the Lorentz factor. By increasing the gap size, the K decreases, which leads to a reduction in the fundamental harmonic wavelength λ_1 and a blue-shift of all the harmonic peaks (blue arrow in Fig. 2). Conversely, decreasing the gap size increases K, which results in an increase in λ_1 and a red-shift (red arrow in Fig. 2) of all the harmonic peaks. Thus, the harmonic peak wavelengths can be tuned by adjusting the gap size within the range of K values (see Table 1 for the K value range).

Figure 3a shows the on-axis flux (in photons/s/0.1%-bandwidth) of the harmonic peaks in the tunable range for three IVU types at Korea-4GSR. A maximum brightness of 10^{15} photons/s/0.1%-bandwidth is attained at photon energies below 9.7 keV for IVU24, and below 11 keV for IVU20 and IVU22. The flux then decreases with increasing photon energy, crossing 10^{14} photons/s/0.1%-bandwidth at 36 keV for IVU20, and 37 keV for IVU22 and IVU24. At higher

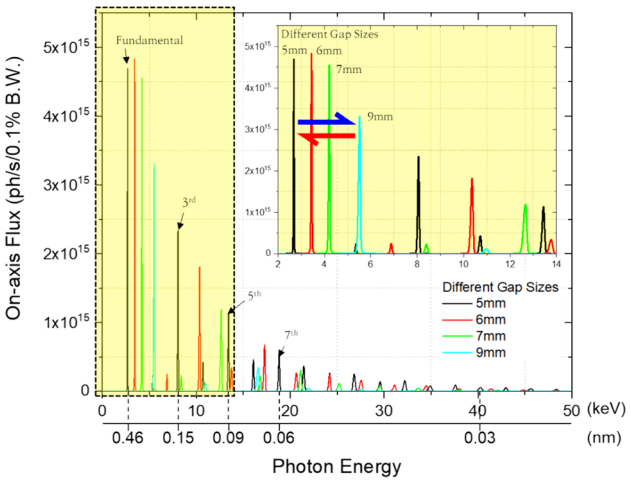

Fig. 2 The on-axis spectra of IVU20 generated with different gap sizes. An aperture with dimensions of 1 mm × 1 mm, located 32 m from the source, is assumed. As the gap size increases, the harmonic peaks exhibit a blue shift (indicated by the blue arrow), while a red shift occurs with a decrease in the gap size (indicated in the red arrow)

photon energies, the flux falls below 10^{13} photons/s/0.1%-bandwidth at: 62 keV for IVU20, 63 keV for IVU22, and 66 keV for IVU24.

In Fig. 3b, the brightness of the three IVUs is compared. Normalized to the brightness of IVU20, the curves for IVU22 and IVU24 fluctuate but exhibit an overall upward trend with increasing photon energy. Below 15 keV, IVU20 is generally brighter than IVU22 and IVU24. At photon energies of 5, 10, and 15 keV, the brightness of IVU24 is 73, 75, and 80%, respectively, compared to that of IVU20.

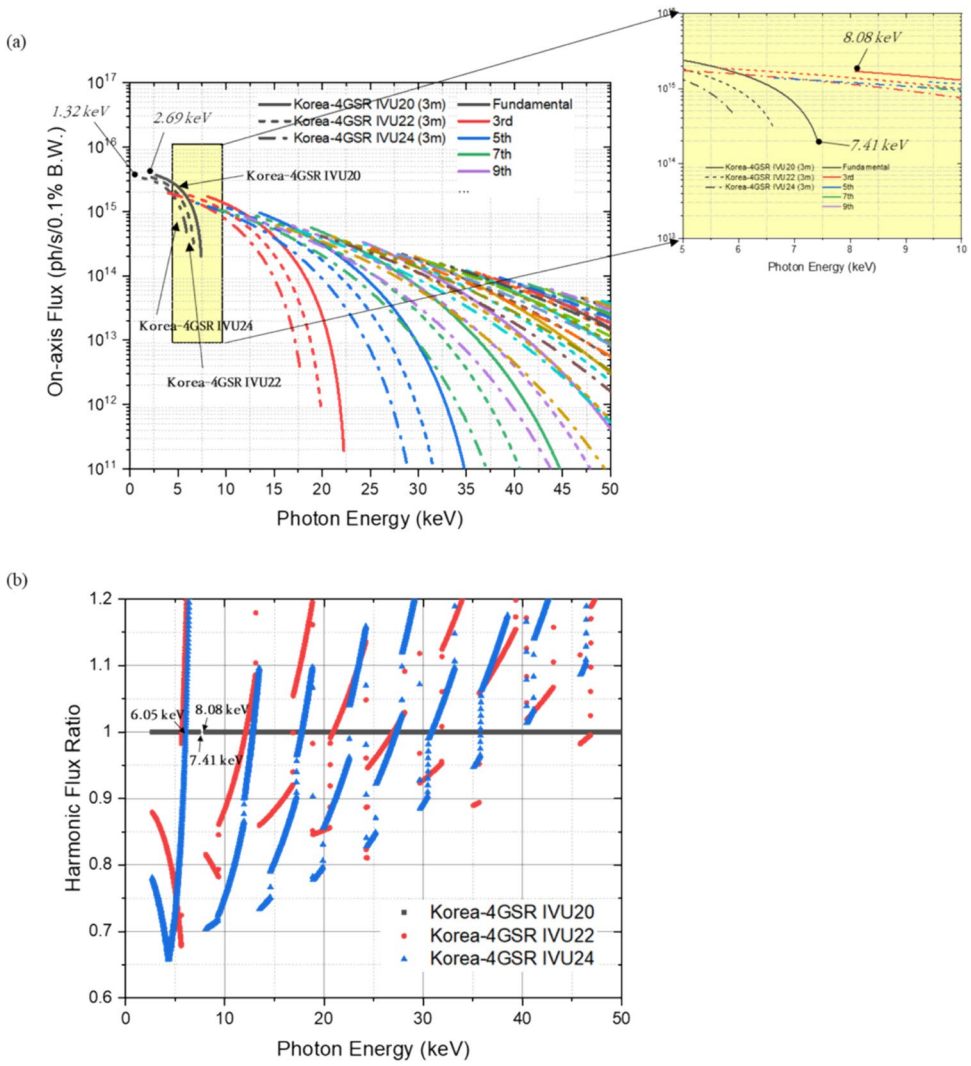

Fig. 3 Comparison of the on-axis flux of the harmonic peaks among the three IVU types at Korea-4GSR. **a** The on-axis flux. Inset: the spectral discontinuity of IVU20 between 7.41 and 8.08 keV. **b** Brightness normalized with respect to IVU20, calculated for only the most intense harmonics in (**a**)

IVU22 is slightly brighter: 76, 88, and 88% of IVU20's brightness at the respective energy levels. Above 30 keV, both IVU22 and IVU24 surpass the brightness of IVU20. Notably, the brightness of IVU24 exhibits a faster rate of increase compared to IVU22.

The minimum photon energy with IVU20 is 2.69 keV. Additionally, it features a spectral gap between 7.41 and 8.08 keV, where no harmonics are present (see Fig. 3a inset). Below the gap, spanning from 6 to 7.41 keV, the fundamental harmonic of IVU20 sharply declines without the presence of additional harmonics. In contrast, IVU22 and IVU24 lack spectral gaps as the tail of their first harmonic is overlapped by their third harmonic. The minimum photon energy with IVU22 is 1.88 keV; that with IVU24 is 1.32 keV.

We calculated the source size and angular divergence of the photon beam for the three IVU types using Eqs. (5) and (6). Given their dependence on global parameters of ε and β, as well as the common parameter L and the sole independent variable λ_n, their values are expected to be uniform among the IVU types and exhibit continuity as a function of λ_n.

At Korea-4GSR, the horizontal electron beam size σ_x is 19 μm, which is 17 times smaller than at PLS-II (see Table 2). Despite its diminutive size, it is still larger than the inherent photon beam size σ_r, which is 4.0 μm at 3 keV and diminishes to 1.5 μm at 20 keV (calculated using Eq. (3)). Consequently, the electron beam size dominates the convoluted source size Σ_x, which shrinks by 5% and converges to σ_x as photon energy increases (Fig. 3a). On the other hand, the vertical electron beam size σ_y is 4.0 μm (see Table 2), comparable to the inherent photon beam size σ_r. The convoluted source size in the vertical direction Σ_y is, thus, responsive to the changes in σ_r, decreasing by 40% before converging to σ_y at higher photon energies (Fig. 3b).

The electron beam divergences at Korea-4GSR, $\sigma_{x'}$ at 3.0 μrad and $\sigma_{y'}$ at 1.4 μrad (see Table 2), are even smaller than the inherent photon beam divergence $\sigma_{r'}$, which is 8.3 μrad at 3 keV and diminishes to 3.2 μrad at 20 keV (calculated

using Eq. (4)). Therefore, the convoluted angular divergence values $\Sigma_{x'}$ and $\Sigma_{y'}$ are predominantly influenced by $\sigma_{r'}$. Interestingly, their curves are not continuous but fluctuate as the harmonic number changes, as shown in Fig. 4c and d. This variability indicates the onset of the electron energy spread effect, which has been omitted in Eqs. (3) and (4). While this exclusion is suitable for third-generation strong rings with an emittance of 10^{-8} m•rad [6], it proves inadequate for Korea-4GSR with ε at 62 pm•rad and an electron energy spread of 0.126% (see Table 2). Incorporating the electron energy spread introduces a multiplication factor to Eq. (4), with the independent variable of normalized energy spread σ_ε defined as

$$\sigma_\varepsilon = 2\pi n N \sigma_{\mathrm{E}}, \tag{8}$$

where n is the harmonic number and σ_{E} represents the energy spread of the electron beam, as formulated in Eq. (16) from [6]. IVU20 experiences the greatest impact due to its larger N (see Table 1), which is suggested by the largest broadening of the angular divergence for given n and λ_{n}; on the other hand, IVU24 is the least affected, attributed to its smaller N (see Fig. 4c and d). The angular divergence fluctuates between 6 and 10 μrad for IVU20, rather than converging to the electron beam divergence values (depicted as the zero-energy spread curves in Fig. 4c and d). For IVU22, the angular divergence varies slightly wider, between 6 and 11 μrad, which is attributed to the broader photon energies covered by IVU22 harmonics. Similarly, for IVU24, the divergence range is even wider, spanning from 6 to 12 μrad, reflecting the broader photon energy ranges covered by IVU24 harmonics.

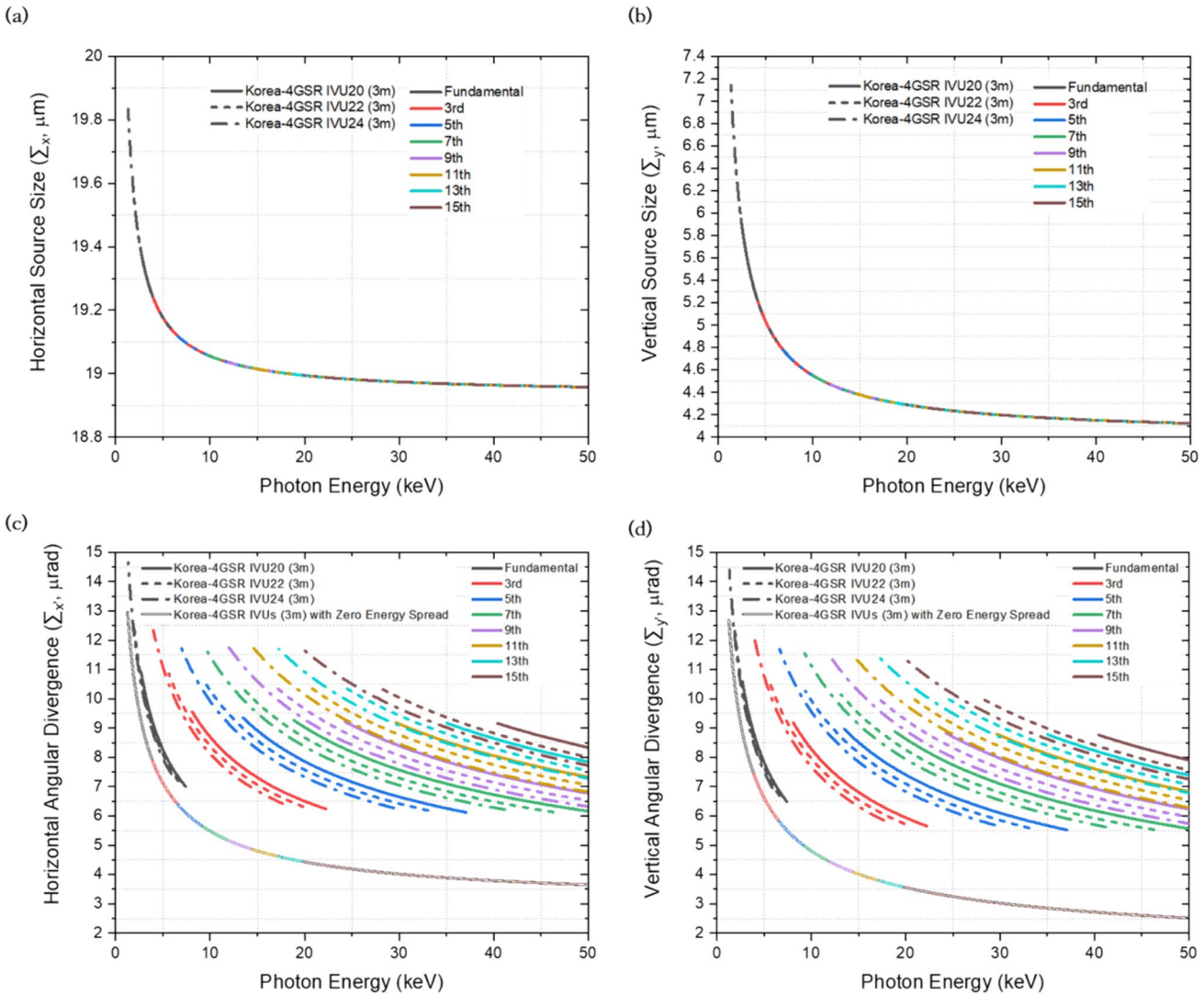

Fig. 4 Comparison of the source size and angular divergence of the photon beams among the three IVU types at Korea-4GSR. **a** Horizontal source size; **b** vertical source size; **c** horizontal angular divergence; **d** vertical angular divergence

The electron energy spread effect on angular divergence of the photon beam becomes pronounced from the third harmonic and beyond, with the deviation from the zero-energy spread value increasing at higher photon energies. At 10 keV, $\Sigma_{x'}$ and $\Sigma_{y'}$ are, respectively, larger by 1.7 and 2.1 folds, on average. By 20 keV, these values rise to around 2.2 and 2.6, respectively (see Fig. 4c and d). On the other hand, the source size is minimally affected by electron energy spread (see Fig. 4a and b). A deviation from the zero-energy spread value was noted with changes in harmonic number, but remained negligible (data not shown).

Coherent fraction F is a measure of how much smaller the electron beam's size and divergence are compared to those of the inherent photon beam. It approaches 1 when both $\sigma_{x,y}$ and $\sigma_{x',y'}$ are significantly smaller than σ_r and $\sigma_{r'}$, respectively. We decoupled the Eq. (7) into the two directional components (x and y) to calculate coherent fraction for the corresponding horizontal and vertical directions.

As shown in Fig. 5a and b, the coherent fraction values are discrete across different harmonics, because the denominator contains the angular divergence of the photon beam, which is also discrete across different harmonics (see Fig. 4c and d). Again, the discretization of coherent fraction values by the harmonic number n results from the electron energy spread effect; otherwise, coherent fraction should have been identical across the IVU types. Given its larger N, IVU20 is the most affected with its coherent fraction being 6–8% smaller compared to IVU24 (see Eq. (8)).

The diminishing trend of the coherent fraction curves is attributed to the wavelength dependence in Eq. (7): the wavelength is inversely proportional to the photon energy, exerting a stronger influence than the relatively minor changes observed in both source size and angular divergence as photon energies increase. To put it differently, coherent fraction unavoidably declines at higher photon energies. Furthermore, the degradation is exacerbated as the electron energy spread effect becomes more pronounced from the third harmonic onwards.

At 2 keV, the coherent fraction is approximately 0.2 horizontally and 0.7 vertically. At 10 keV, the most commonly used photon energy for coherent studies, it decreases to 0.06 horizontally and 0.3 vertically. To produce a fully coherent beam, the beam must be cropped to leave only 6% of the horizontal size and 30% of the vertical size.

By multiplying the coherent fraction with the on-axis flux, the coherent flux was calculated (Fig. 5c). A maximum coherent flux of 10^{14} photons/s/0.1%-bandwidth is attained at photon energies below 5.7 keV for IVU20, below 5.2 keV for IVU22, and below 4.8 keV for IVU24. The flux then decreases with increasing photon energy, crossing 10^{13} photons/s/0.1%-bandwidth at 11 keV for IVU24 and IVU22, and 12 keV for IVU20. At higher photon energies, the flux falls below 10^{12} photons/s/0.1%-bandwidth at: 20 keV for IVU24, 21 keV for IVU22, and 22 keV for IVU20. At even higher photon energies, the flux falls below 10^{11} photons/s/0.1%-bandwidth at: 32 keV for IVU24, 35 keV for IVU22, and 37 keV for IVU20.

Between 10 and 30 keV, IVU20 has the highest coherent flux, and IVU22 and IVU24 maintain approximately 77% and 60% of IVU20's coherent flux, respectively (Fig. 5d). However, between 7.41 and 8.08 keV, IVU20 is missing the spectral continuity. From 6.8 to 7.41 keV, where the first harmonic of IVU20 diminishes and no additional backup harmonics are present, IVU22 and IVU24 exhibit higher coherent flux due to their third harmonic (see Fig. 5c inset). At a lower photon energy segment, between 3 keV and 6 keV, IVU20 is again the brightest in coherent flux: the coherent flux of IVU22 and IVU24 decreases from 91% to 61% and 83% to 50%, respectively, in comparison to IVU20, as the photon energy increases. In summary, IVU20 emerges as the most coherent overall, except in a photon energy segment between 6.8 and 8.08 keV. The compromised coherent fraction due to the electron energy spread effect (see Fig. 5a and b) is offset by the higher on-axis flux of IVU20 (see Fig. 3).

Lastly, the total radiation power for the three IVU types at Korea-4GSR was calculated using

$$P_T = 0.633E^2[\mathrm{GeV}]B_0^2[\mathrm{T}]L[\mathrm{m}]I[\mathrm{A}] \tag{9}$$

$$\propto E^2\left(\frac{K}{\lambda_u}\right)^2 \mathrm{LI}$$

in which contributions from all harmonics and their on- and off-axis components are included [12]. This differs from the on-axis flux shown in Figs. 2 and 3, which only accounts for the odd harmonics within the central cone radiation. Total radiation power provides an indication of how much extra heat should be managed at the beamline. For IVU20, this power ranges from 12.5 kW at the minimum gap size of 5 mm to 0.17 kW at the maximum gap size of 18 mm. For IVU22, it ranges from 15.2 kW at the minimum gap size to 0.25 kW at the maximum gap size. As for IVU24, the total power ranges from 17.9 kW at the minimum gap size to 0.36 kW at the minimum gap size (Fig. 6).

On the other hand, the power of on-axis flux or central cone radiation, calculated as the central flux within four times the inherent photon beam divergence $\sigma_{r'}$ [7], constituted only a small fraction of the total radiation power. This ranged, for IVU20, from 0.20 kW at the minimum gap size to 0.0040 kW at the maximum gap size; for IVU22, from 0.29 kW at the minimum gap size to 0.0064 kW at the maximum gap size; and for IVU24, from 0.41 kW at the minimum gap size to 0.095 kW at the maximum gap size. The efficiency through the gap size variation averaged at 1.95,

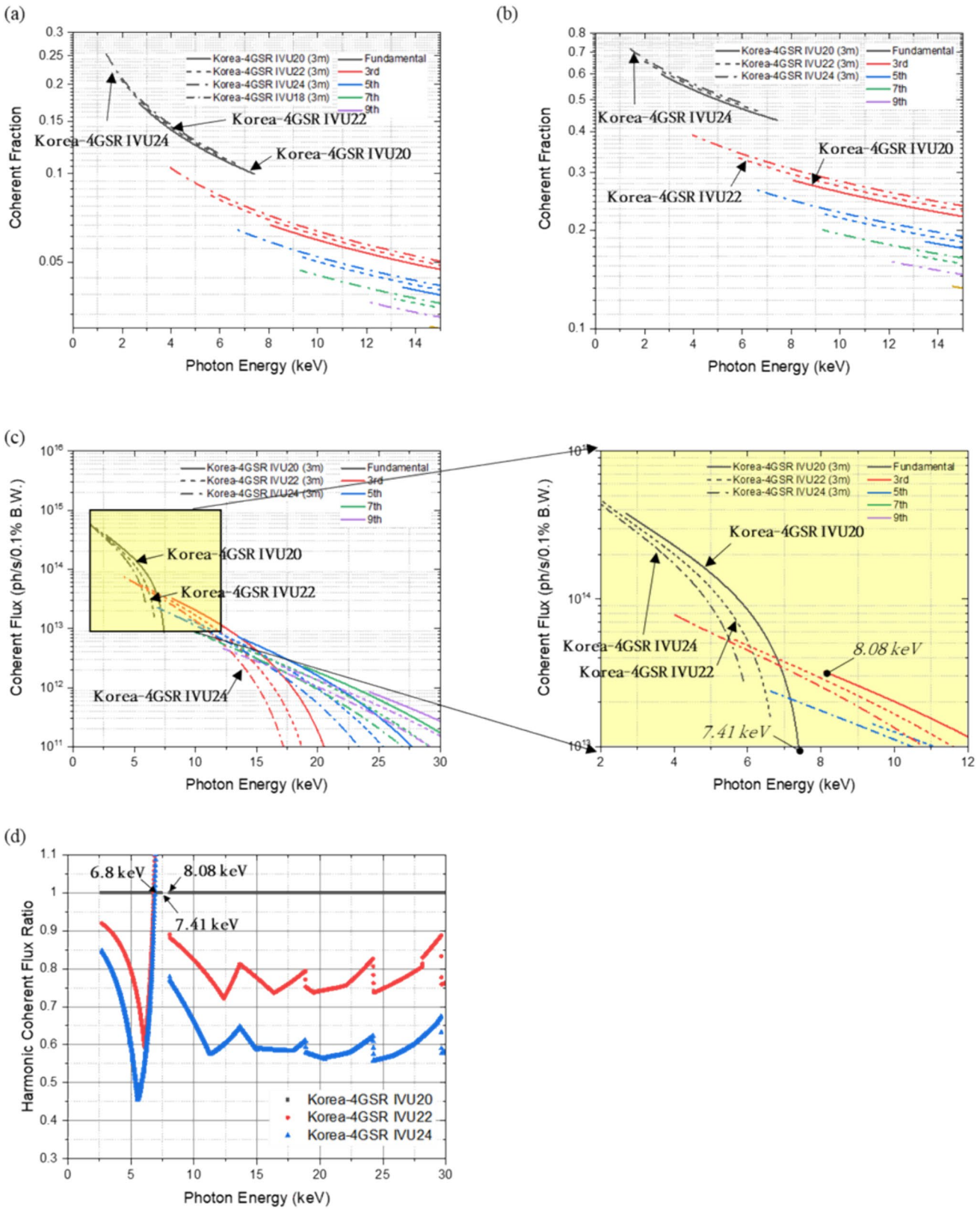

Fig. 5 Comparison of the coherent fraction and the coherent flux among the three IVU types at Korea-4GSR. **a** Horizontal coherent fraction; **b** vertical coherent fraction; **c** coherent flux. Inset: the loss of coherency flux dominance exhibited by IVU20 within the photon energy range of 6.8 to 8.08 keV; **d** coherent flux normalized with respect to IVU20

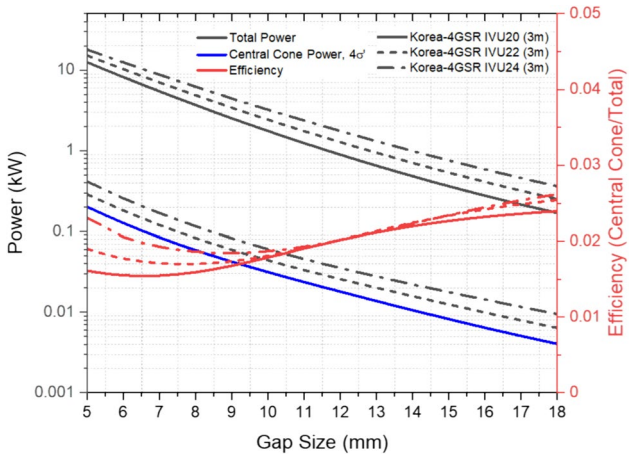

Fig. 6 Total radiation power and the central cone radiation power. The central cone radiation is defined as the central flux within four times the inherent photon beam divergence $\sigma_{r'}$ [7]. The efficiency is then calculated as the ratio of the central cone radiation power to the total radiation power

2.04, and 2.14% for IVU20, IVU22, and IVU24, respectively. Only this on-axis flux is channeled into the beamline, while excessive off-axis radiation is blocked using cooled masks. APS reports managing up to 21 kW of the total radiation power in its beamlines [13].

Operating the undulator with a small K offers advantages in reducing total radiation power (see Eq. (9)) and decreasing photon beam divergence (see Eq. (4) and Fig. 4c and d), thereby, enhancing beam coherence. Additionally, a relatively large gap size is beneficial for both mechanically controlling the gap size and safely maneuvering the electron beam orbit through the gap. However, the spectral coverage of individual harmonics contracts on the lower photon energy side, potentially limiting spectral continuity. The first phase hard X-ray beamlines at Korea-4GSR choose to cover a wider spectral range because it is difficult to predict which photon energy will emerge as dominant in the future for each of the beamlines. As users gain experience and identify strong applications, discussions on spectral specialization for more efficient undulator design will follow.

Table 3 is a recommendation table based on the assessment of the photon beam characteristics for the three IVUs at Korea-4GSR. Peak brightness levels are comparable, exhibiting fluctuations within a range of ± 30%. IVU20 is the brightest overall at photon energies below 15 keV, while IVU24 is advantageous above 30 keV; IVU22 holds an intermediate position (see Fig. 3b). For coherent applications, IVU20 is the brightest; the coherence flux for IVU22 and IVU24 is 77% and 60%, respectively, compared to IVU20, in the 10 keV to 30 keV range (Fig. 5d). However, IVU20 exhibits a compromised or missing spectral range between 6.8 keV and 8.08 keV. IVU22 maintains spectral continuity with a minimal gap size of 5.58 mm, while IVU24 offers a larger margin with a minimal gap size of 6.46 mm (data not shown). IVU24 is a practical choice for a beamline requiring frequent gap size adjustments.

Finally, the performance of IVU20 at Korea-4GSR was assessed compared to the PLS-II undulator and the U21 undulator at APS-U. As shown in Fig. 7a, the on-axis flux of IVU20 is approximately ten times higher than that of the PLS-II undulator between 10 and 15 kV, and approximately 20 times higher at 20 keV. This gap continues to widen at higher photon energies, with IVU20 being 50 times brighter at 30 keV. The increased brightness results from the elevated electron energy from 3 to 4 GeV and the extended undulator length from 1.3 to 3.0 m at Korea-4GSR (see Table 1). The on-axis flux is comparable to that of U21 at APS-U. The significant spectral gap noted for the APS-U undulator is attributed to its limited K value range, which remains below 1.2 (see Table 2).

According to the comparison in Fig. 7b, the coherent flux at Korea-4GSR is even higher than that of PLS-II. The 100 times smaller emittance at Korea-4GSR reduces both the electron beam size and the electron beam divergence, resulting in 1000 times increase in coherent flux at below 10 keV. The gap continues to widen at higher photon energies, with 3000 times higher coherent flux at 15 keV and 6000 times higher at 20 keV.

Oh et al. had proposed a scheme to achieve a coherent fraction of 0.3 at Korea-4GSR by optimizing the beta (β) function for phase-space matching between electron and

Table 3 Comparison of the three IVU types at Korea-4GSR based on their photon beam characteristics

IVU type	IVU20	IVU22	IVU24
On-axis flux	Comparable, exhibiting fluctuations within a range of ± 30%		
	Good below 15 keV	intermediate	Good above 30 keV
Coherent flux	Best	77% of IVU20's between 10 and 30 keV	60% of IVU20's between 10 and 30 keV
Spectral continuity	Missing/compromised between 6.8 keV and 8.08 keV	Perfect with the minimum gap size < 5.58 mm	Perfect with the minimum gap size < 6.46 mm
Max total power by off-axis radiation	Best: 12.5 kW at the minimum gap size	15.2 kW at the minimum gap size	17.9 kW at the minimum gap size

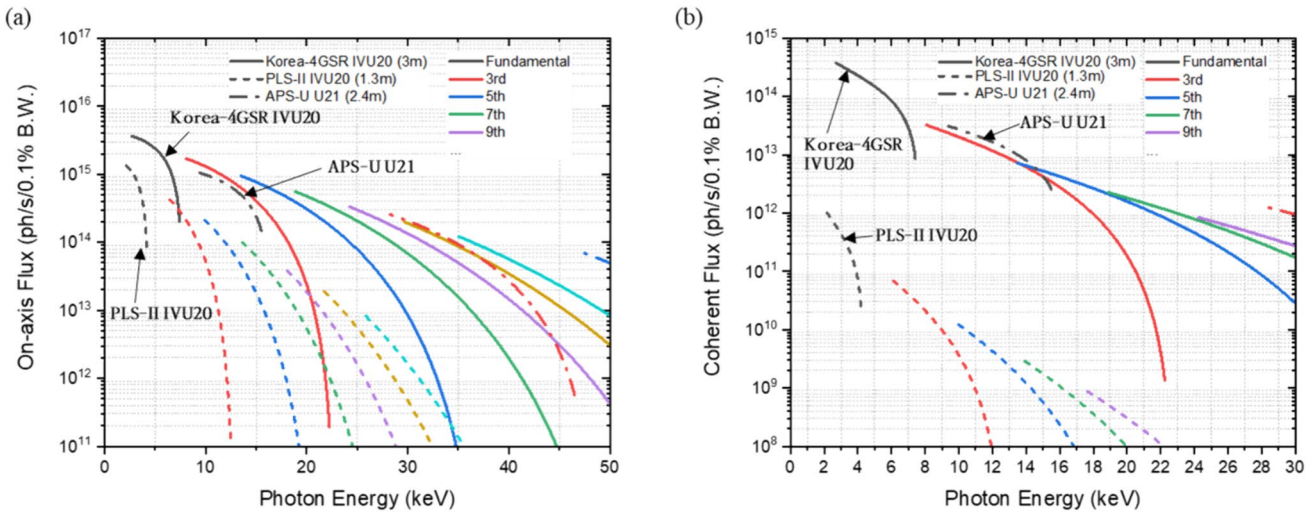

Fig. 7 Comparison of IVU20 at Korea-4GSR with the PLS-II undulator and the U21 undulator at APS-U. **a** On-axis flux; **b** the coherent flux

photon beams [8], which has not been adopted in the latest machine parameters of Korea-4GSR (see Table 2). Yet, the predicted increase in coherent flux is still remarkable. Additionally, the coherent flux is comparable to that of U21 at APS-U, which shares similar electron beam size and electron beam divergence (see Table 2).

3 Conclusion

The target emittance of Korea-4GSR below 100 pm rad is unprecedented in South Korean scientific history and also stands out globally as no synchrotron facilities worldwide currently operate with such a low emittance value. We have presented the calculated photon beam characteristics of the hard X-rays from the IVUs designated for the first phase beamlines at Korea-4GSR. The ultra-low emittance significantly reduces the electron contribution to the source size and angular divergence of the photon beam, resulting in a predicted source size of 19–20 μm horizontally and 4–7 μm vertically, with an angular divergence between 6 and 12 μrad. This leads to a remarkable improvement in beam coherence, surpassing the coherence flux of PLS-II by over 1000-fold. The on-axis photon flux undergoes a 10–20-fold increase, primarily due to the elevated electron energy and the extended undulator length at Korea-4GSR.

The brightness is comparable among the three variants of IVUs: IVU20, IVU22, and IVU24. IVU20 exhibits the highest coherence but lacks dominance in a segment of the spectrum between 6.8 and 8.08 keV. IVU22 and IVU24, while moderately inferior in coherent flux compared to IVU20, ensure spectral continuity. IVU24 provides a wider gap size margin for spectral continuity and is suitable for beamlines requiring frequent gap size adjustments. However, as the total radiation power reaches up to 17.9 kW with IVU24, proper mask design with efficient cooling is crucial to selectively transmit the on-axis beam. In contrast, IVU20 is the least thermal, with a total radiation power of 12.5 kW. IVU22 falls in between the two IVU types.

Unexpectedly, we have noted that the electron beam energy spread effect cannot be ignored when employing undulators at Korea-4GSR. This aligns with the condition described in [6], where the emittance is by far small for the level of electron beam energy spread. The effect significantly contributed to an increase in the angular divergence of the photon beam, thus compromising beam coherence. This phenomenon was particularly noticeable from the third harmonic onwards, and its impact was more pronounced for undulators with larger n and higher K values (see Fig. 4c and d). Consequently, longer IVUs are expected to be more susceptible to this compromise, deviating more substantially from the anticipated performance.

The presented photon beam characteristics are indispensable for designing the optics of individual beamlines, including the selection of the IVU type. During commissioning, the source, optics, and their alignment will be evaluated based on this information. Additionally, it will serve as a reference for designing future undulators with enhanced performance.

Acknowledgements The authors would like to express their gratitude to Drs. Jaeyu Lee and Jaeyong Shin of the 4GSR Project Headquarters for their discussions regarding undulator radiation. This work was supported by the Korean Ministry of Science and ICT (MSIT) under grant number RS-2022-00155836 for the Multipurpose Synchrotron Radiation Construction Project and by the Pohang Accelerator Laboratory, which receives support from MSIT and POSTECH.

References

1. Y. Lee, E. Kim, J. Kim, J. Lee, J. Hwang, S. Shin, G. Jang, S. Park, J. Seok, Conference Proceeding, 14th International Particle Accelerator Conference, Venice, Italy, pp. 1128–1130 (2023) https://doi.org/10.18429/JACoW-IPAC2023-MOPM060
2. J. Doucet, Nucl. Instrum. Methods Phys. Res., Sect. B **199**, 10–14 (2003)
3. Y. Watanabe, Synchrotron Radiat. News **20**, 40–44 (2007)
4. APS-U, The Advanced Photon Source, https://www.aps.anl.gov/Beamline-Selection/Technical-Information. Accessed 15 Mar 2024
5. P. Raimondi, C. Benabderrahmane, P. Berkvens, J.C. Biasci, P. Borowiec, J.-F. Bouteille, T. Brochard, N.B. Brookes, N. Carmignani, L.R. Carver, J.-M. Chaize, J. Chavanne, S. Checchia, Y. Chushkin, F. Cianciosi, M. Di Michiel, R. Dimper, A. D'Elia, D. Einfeld, F. Ewald, L. Farvacque, L. Goirand, L. Hardy, J. Jacob, L. Jolly, M. Krisch, G. Le Bec, I. Leconte, S.M. Liuzzo, C. Maccarrone, T. Marchial, D. Martin, M. Mezouar, C. Nevo, T. Perron, E. Plouviez, H. Reichert, P. Renaud, J.-L. Revol, B. Roche, K.-B. Scheidt, V. Serriere, F. Sette, J. Susini, L. Torino, R. Versteegen, S. White, F. Zontone, Commun. Phys. **6**, 82 (2023)
6. T. Tanaka, H. Kitamura, J. Synchrotron Radiat. **16**, 380–386 (2009)
7. D. Attwood, Soft X-Rays and Extreme Ultraviolet Radiation: Principles and Applications (Cambridge University Press, Cambridge, 1999)
8. B. Oh, J. Ko, J. Lee, G. Jang, S. Shin, Appl. Sci. **11**, 24 (2021)
9. V. Smaluk, R. Fielder, A. Blednykh, G. Rehm, R. Bartolini, Phys. Rev. Accel. Beams **17**, 074402 (2014)
10. T. Tanaka, J. Synchrotron Radiat. **28**, 1267–1272 (2021)
11. T. Tanaka, H. Kitamura, J. Synchrotron Radiat. **8**, 1221–1228 (2001)
12. A.C. Thompson, D. Vaughan, Center for X-ray Optics Advanced Light Source: X-ray Data Booklet, 2nd edn. (Lawrence Berkeley National Laboratory, University of California, Berkeley, California, 2001), https://cxro.lbl.gov/x-ray-data-booklet
13. Y. Jaski, M. Abliz, J.S. Downey, S.H. Lee, J. Mulvey, S.M. Oprondek, M. Ramanathan, F. Westferro, B.X. Yang, Conference Proceeding, Mechanical Eng. Design of Synchrotron Radiation Equipment and Instrumentation (MEDSI2018), Paris, France, pp. 388–390 (2018) https://doi.org/10.18429/JACoW-MEDSI2018-THPH24